Cancer-derived exosomal-Alu RNA promotes colorectal cancer progression

Valeria Tarallo

valeria.tarallo@igb.cnr.it

Institute of Genetics and Biophysics 'Adriano Buzzati Traverso', CNR https://orcid.org/0000-0002-6920-4402

Sara Magliacane Trotta

Institute of Genetics and Biophysics 'Adriano Buzzati Traverso', CNR

Antonio Adinolfi

Institute of Genetics and Biophysics 'Adriano Buzzati Traverso', CNR

Luca D'Orsi

Institute of Genetics and Biophysics 'Adriano Buzzati Traverso', CNR

Sonia Panico

Institute of Genetics and Biophysics 'Adriano Buzzati Traverso', CNR

Grazia Mercadante

Institute of Genetics and Biophysics 'Adriano Buzzati Traverso', CNR

Patrick Mehlen

Centre de Recherche en Cancérologie de Lyon, INSERM U1052-CNRS UMR5286, Université de Lyon, Centre Léon Bérard

Jayakrishna Ambati

University of Virginia School of Medicine

Sandro De Falco

Institute of Genetics and Biophysics https://orcid.org/0000-0002-6501-1697

Article

Keywords: Alu RNA, colorectal cancer, exosome, NLRP3 inflammasome, EMT

Posted Date: August 23rd, 2023

DOI: https://doi.org/10.21203/rs.3.rs-3170776/v1

Additional Declarations: (Not answered)

Version of Record: A version of this preprint was published at Experimental & Molecular Medicine on March 14th, 2024. See the published version at https://doi.org/10.1038/s12276-024-01166-6.

Abstract

Inflammation plays a crucial role in cancer progression, but the relevance of the NLRP3 inflammasome remains unclear. *Alu* RNA is the first endogenous nucleic acid identified to activate the NLRP3 inflammasome. Here we show that *Alu* RNA can induce epithelial-to-mesenchymal transition (EMT) through NLRP3 inflammasome activation and releasing IL-1b in colorectal cancer (CRC) cells. *Alu* RNA is stored, transported and transferred to CRC cells by exosomes. Exosomal-*Alu* RNA promotes tumorigenesis by inducing invasion, metastasis and EMT through NLRP3 inflammasome activation. Corroborating this data, we found that the significantly increased expression of *Alu* RNA correlates with the induction of NLRP3 priming in human CRC patients. Furthermore, the expression level of *Alu* RNA from circulating exosomes correlate with CRC progression in preclinical model. These findings reveal the direct involvement of *Alu* RNA in cancer pathogenesis and their presence in CRC cell-derived exosomes could be used as non-invasive diagnostic biomarker.

Introduction

Alu elements are among the most abundant interspersed repetitive elements in human genome, comprising almost 11% of the entire nuclear DNA [1] and at the time of their discovery, they were considered as junk DNA. A typical *Alu* element is approximatively 300 nucleotides in length and does not encode for any proteins. However, it can be transcribed either by RNA Pol II as a part of other transcripts, known as embedded *Alu*, or by RNA Pol III, known as free *Alu* RNAs. While the role of embedded *Alu* is widely studied, as they can cause human disorders through insertional mutagenesis in several genes, the role of free *Alu* RNAs is less known [2]. Free *Alu* RNAs are expressed at very low levels but can accumulate in response to cellular stress and malignant transformation, indicating how they could have a crucial role in pathological context [3,4].

In 2011, we demonstrated that free *Alu* RNAs can cause a human disorder, geographic atrophy, an advanced and untreatable form of age-related macular degeneration that causes blindness in millions of individuals [5]. The accumulation of *Alu* RNA in the retinal-pigmented epithelium (RPE) of human eyes induces cell death and degeneration through the activation of nucleotide-binding domain leucine-rich repeat containing 3 (NLRP3) inflammasome. This is an innate immune complex that senses pattern/danger-associated molecular patterns, resulting in interleukin-18 production and consequent RPE cell degeneration [6]. Since this discovery, a specific role of *Alu* elements have been found in other human disorders, such as systemic lupus erythematosus [7], type II diabetes [8] and Alzheimer's disease [9], but their role in cancer is still the subject of debate. It has been suggested that *Alu* elements have an anti-tumor effect since they induce cytotoxicity in several cancer cells lines [10,11]. Furthermore, a more recent report suggests that they can also confer cancer resistance [12]. Despite these observations, hypomethylation of *Alu* elements has been reported in several cancers, and free *Alu* RNAs have been found accumulated in hepatocellular carcinoma [13]. Moreover, we recently demonstrated that *Alu* expression correlates with tumor growth and metastasis in human colorectal cancer (CRC) patients and triggers epithelial-to-

mesenchymal transition (EMT) in several cancer cell lines [14], suggesting that *Alu* transcripts have a pro-tumoral role in cancer. In line with these reports, tumor macrovesicles isolated from cancer-affected patients has been found to be remarkably enriched in *Alu* transcripts [15].

Alu RNA is the first endogenous nucleic acid described to activate NLRP3 inflammasome, by which it induces RPE cell death [6]. *Alu* RNA has been also found to induce inflammasome activation in other cell types, such as human monocytic leukemia cells (THP-1) and human cervical cancer cells (HeLa) [6], suggesting that the inflammasome machinery can be activated in cancer cells. The activation of inflammasome in cancer is controversial, being described to either positively affect cell-autonomous death pathways and anticancer surveillance or stimulate autocrine and paracrine processes promoting tumor growth and metastasis [16]. The basal levels of NLRP3 expression are not typically sufficient for NLRP3 inflammasome activation. Therefore, a two-step process of priming and activation is required. Priming refers to the upregulation of the transcription of *NLRP3* as well as the pro-form of the inflammatory cytokines *IL1B* and *IL18*. Subsequently, the activation step induces the autoproteolysis of Pro-caspase-1 into its cleaved and active fragment [17]. Although it has been shown that NLRP3 is associated with EMT in CRC patients [18,19] and several reports have correlated the secretion of IL-1b with EMT, tumor progression and metastasis [20–22], the underlying molecular mechanism in CRC remains unknown.

Here we demonstrate that *Alu* RNA induces EMT in CRC cell lines by activating the NLRP3 inflammasome and releasing IL-1b. We also show that *Alu* RNA is stored and transported by exosomes and that CRC-derived exosomal-*Alu* RNA can be transferred to cancer cells, thus promoting cancer progression by inducing EMT through NLRP3 inflammasome activation. Finally, our preclinical data suggest that *Alu* RNA from circulating exosomes could be potentially used as biomarkers for CRC diagnosis.

Materials and Methods

Cell culture

All cancer cell lines were purchased from ATCC and were cultured at 37°C in the presence of 5% CO_2. The human colon cancer (HCT116 and HT-29) cell lines were grown in McCoy's 5A Medium. The human colon cancer (SW480 and LS174T), the human breast cancer (MCF7) and the human cervix cancer (HeLa) cell lines were grown in Dulbecco Modified Eagle Medium. The human kidney carcinoma (A498) cell line was grown in Eagle's Minimum Essential Medium. The human lung cancer (H460) cell line was grown in RPMI-1640 Medium. Each medium was supplemented with 10% heat-inactivated fetal bovine serum (FBS), 2 mM glutamine and standard concentration of antibiotics (EuroClone). For OLT1177 dapansutrile (Merck - Sigma-Aldrich) treatment, the cells were treated with 100μM in the complete medium.

Human tissues

Human primary colorectal cancer, colorectal cancer liver metastasis and their corresponding adjacent normal snap-frozen tissue samples were obtained from the Biological Resources Center (CRB, Centre de Resource Biologique) of Centre Léon Bérard (protocol number: BB-0033-00050) (Lyon, France). Protocol using human material was approved by the CRB medical and scientific committee. All patients signed informed consent to participate to research according to the French laws. RNA from human tissues was extracted QIACUBE kit (Qiagen), following manufacture's protocol. RNA concentration was measured by Nanodrop system (Thermoscientific) and RNA quality was evaluated by TapeStation system (Life Tecnhologies).

In Vitro Transcription of Alu RNA

We synthesized a 281 nucleotides *Alu* RNA sequence originating from the cDNA clone TS 103, which is known to be expressed in human cell (Shaik et al., 1997). The pT7/*Alu* plasmid was linearized with DraI and subjected to HiScribe T7 Quick High Yield RNA Synthesis Kit (BioLabs), according to the manufacturer's instructions. After the T7 transcription reaction, RNA was treated with DNase and purified following phenol–chlorophorm extraction and ethanol precipitation. RNA was quantified at Nanodrop and the integrity was monitored by gel electrophoresis. This yields single-stranded RNA that fold into a defined secondary structure identical to Pol III derived transcripts.

Transient transfection

Cells were transfected with *Alu* RNA, or *siNLRP3* 5'-GUUUGACUAUCUGUUCUdTdT-3' and *siLuc* 5'-UAAGGCUAUGAAGAGAUdTdT-3' (control for *siNLRP3*) using Lipofectamine 2000 (Invitrogen), according to the manufacturer's instructions.

Cell viability

Cell viability were assessed using the CellTiter 96 Aqueous One Solution Cell Proliferation Assay or Cell Titer-Glo® Luminiscent assay (Promega) according to the manufacturer's instructions.

ELISA

IL-1β secretion in conditioned cell culture media was analyzed using the Human IL-1β ELISA Kit (Abcam) according to the manufacturer's instructions.

Caspase-1 activation assay

Caspase-1 activity was measured using the Cell Meter Live Cell Caspase-1 Binding Assay Kit - Green Fluorescence - (AAT Bioquest, Inc.), according to the manufacturer's instructions.

Exosomes purification, characterization and treatment

Exosomes were purified from CRC-derived conditional or serum of CRC-xenotrasplanted mice by ultracentrifugation. After transfection, CRC were cultured in Dulbecco Modified Eagle Medium supplemented with 5% fetal bovine serum (FBS) exosomes-depleted. FBS was depleted of bovine exosomes by ultracentrifugation at 100,000 x g for 70 minutes. After 72 hours of incubation, the

conditioned media was collected and centrifuged at 2,000 x g for 30 minutes to eliminate cells and debris. The supernatant was ultracentrifuged by SW41Ti rotor at 14,000 x g for 30 minutes and then at 100,000 x g for 70 minutes. Exosomes were washed with phosphate-buffered saline (PBS) and collected by ultracentrifugation at 100,000 x g for 70 minutes. For transmission electron microscopy, exosomes were fixed in 2% Glutaraldeyde. The sample was applied to formvar/carbon 100-mesh grids and incubated for 10 min. Grids were washed twice with filtered distilled water and stained using 1,5% UA in water for 10 min. After they were washed with water to remove the excess staining solution and grids were air-dried. Images were acquired from grids using a FEI Tecnai 12 transmission electron microscope (FEI Company, Hillsboro, Oregon, USA) equipped with a Veleta CCD digital camera (Olympus Soft Imaging Solutions GmbH, Münster, Germany) and operating at 120 kV. For exosome-tracking experiments, purified exosomes were labeled using PKH67 Green Fluorescent Cell Linker Mini Kit for membrane dye (Merck - Sigma-Aldrich) according to the manufacturer's instructions. Exosomes from single mouse serum were purified using Total Exosomes Isolation Kit (from plasma) (Invitrogen) according to manufacturer's instructions.

Western blot analysis

Cell lines were preparated with lysis buffer (Tris-HCl 20 mM pH 8, NaCl 150 mM, Triton X-100 1%, EDTA 10 mM, Glycerol 10%, ZnAc 1mM), separated by SDS-polyacrylamide gel electrophoresis, transferred to polyvinylidene difluoride membranes (Amersham Biosciences) and probed with the following antibodies: Fibronectin (Merck - Sigma-Aldrich, 1:1,000), Vimentin (Cell Signaling, 1:1,000), ZEB1 (Atlas Laboratories, 1:1,000), Cleaved Caspase-3 (Cell Signaling, 1:1,000), Cleaved Caspase-1(p20 fragment, AdipoGen, 1:1,000), CD63 (Thermo Scientific, 1:500), antibody mouse polyclonal E-Cadherin (Cell Signaling, 1:1,000). For the normalization we used an antibody against β-Tubulin (Elabioscience, 1:2,000) or Vinculin (Cell Signaling, 1:10,000). The secondary antibody, goat anti-rabbit (GeneTex) or anti-mouse HRP (ImmunoReagents) was diluted 1: 10,000. The signals were visualized by chemiluminescence using ECL substrate (Advansta) or extra sensitive chemiluminescence using LiteAblot Turbo (EuroClone), following manufacturer's instructions.

Quantitative reverse transcriptase PCR

Total RNA from cells and exosomes was extracted from cells using TRIzol reagent (Invitrogen) according to manufacturer's recommendations. Total RNA was reverse transcribed using QuantiTec Reverse Transcription Kit (Qiagen). The RT products (cDNA) were amplified by real-time quantitative PCR (Applied Biosystems 7900 HT Fast Real-Time PCR system) with Power SYBR green Master Mix. Oligonucleotide primers specific for human *18S* rRNA (forward 5'-CGCAGCTAGGAATAATGGAATAGG-3' and reverse 5'-GCCTCAGTTCCGAAAACCAA-3'), *Alu* (forward 5'- CAACATAGTGAAACCCCGTCTCT-3' and reverse 5'-TAGCTGGGACTACAGGCG – 3'), human *NLRP3* (forward 5'-GCACCTGTTGTGCAATCTGAA-3' and reverse 5'-TCCTGACAACATGCTGATGTGA-3'), human *IL-1β* (forward 5'-TTAAAGCCCGCCTGACAGA-3' and reverse 5'-GCGAATGACAGAGGGTTTCTTAG – 3'), human *IL-18* (forward 5'-ATCACTTGCACTCCGGAGGTA-3' and reverse 5'-AGAGCGCAATGGTGCAATC-3'), and human *β- Actin* (forward 5'-CTCTTCCAGCCTTCCTTCCT-3' and reverse 5'-TGTTGGCGTACAGGTCTTTG-3') were used. The qPCR cycling conditions were 50°C for 2

min, 95°C for 10 min followed by 40 cycles of a two-step amplification program (95°C for 15 s and 58°C for 1 min). At the end of the amplification, melting curve analysis was applied using the dissociation protocol from the Sequence Detection system to exclude contamination with unspecific PCR products. The PCR products were also confirmed by agarose gel and showed only one specific band of the predicted size. For negative controls, no RT products were used as templates in the QPCR and verified by the absence of gel-detected bands. Relative expressions of target genes were determined by the $2^{-\Delta\Delta Ct}$ method.

Northern Blot

Total RNA (100–200 ng) was denatured for 10 minutes at 70°C in a Tris-Borate-EDTA buffer–urea 2X loading buffer (BioRad) and then run on a 10% denaturing Tris-Borate-EDTA buffer–urea–polyacrylamide gel. Then the RNA was transferred to a positively charged nylon membrane (Amersham). The membrane was cross-linked by UV irradiation and saturated with a pre-hybridization solution (formamide 50%, sodium phosphate buffer 0.12 M pH 7.2, NaCl 0.25 M, EDTA 1 mM, SDS 7%) at 42°C for 1 hour. 150 ng of denatured *Alu* probe was added and incubated for 16 hours at 42°C. *Alu* probe was obtained by PCR reaction using as template the plasmid p*Alu*, the specific primers (*Alu* probe F: 5'-GGGCCGGGCGCGGTG-3' and *Alu* probe R 5'GTACCTTTAAAGAGACAGAGTCTCGC-3', biotinylated on the 5'-side) and the following cycle: 5 min at 95°C, 1 min at 95°C, 30 s 58°C, 1 min at 72°C for 40 cycles and 8 min at 72°C. The reaction product was then purified using ProbeQuant G-50 Micro Columns (GE Healthcare) following manufacturer instructions. For the normalization, we used a 5'-biotinylated probe against *5S* RNA (5'-AGCCTACAGCACCCGGTATT-3') at final concentration of 1 ng/µl. The membrane was washed twice with 2X SSC, 0.2% SDS at 65°C. For the detection, we used Chemiluminescent Nucleic Acid Detection Module (Thermo Scientific) following the manufacturer's instructions.

Transwell invasion assay

Exosome-treated CRC cells ($1x10^5$) were seeded into the upper chamber of a 24-multiwell insert system with 8 µm pore size polycarbonate filter (Corning) coated with 200 µg/ml of Matrigel. The lower chamber was filled with complete medium for positive control and with medium without serum for negative control. After 24hours, the cells on the top of the filter were removed and those on the bottom side were stained with 4',6-diamidino-2-phenylindole (DAPI). Images were recorded on Nikon Eclipse Ni-E (Nikon, Corporation Tokyo, Japan) fluorescence microscope. For each group, seven random transwell chamber fields were counted. Single cells were counted using ImageJ (NIH, Bethesda, MD, USA).

Soft Agar Assay

Six-well plates were pre-coated with 0.75% basal agar layer with culture media. Exosome-treated CRC cells ($1x10^5$) were re-suspended in 0.32% upper agar layer and seeded at the density of $1.25x10^4$ cells per well. The medium was changed every 3 days. After 15 or 21 days, cell colonies were fixed with 4% PFA and visualized by 0.005% Crystal Violet (Merck - Sigma-Aldrich) staining. Images were captured and the colony number was counted by Image J software (NIH, Bethesda, MD, USA).

Colony Formation Assay

Exosome-treated CRC cells were plated at 500 cells/well in 6-multiwell. After 7 days, cell colonies were visualized by 0.005% Crystal Violet (Merck - Sigma-Aldrich) staining. Images were captured and the colony number was counted by ImageJ software (NIH).

Animals

CD1 mice were purchased from Charles River. Animal experiments were in accordance with European directives no. 2010/63/UE and Italian directives D.L. 26/2014, and were approved by the Italian Ministry of Health (Authorization no. 492/2020-PR of 19/05/2020). For all procedures, 7- to 8-week- old male mice were used and anesthesia was achieved by intraperitoneal injection of 100 mg/kg ketamine hydrochloride and 10 mg/kg xylazine.

Xenograft tumor model

$3x10^6$ of HCT116 cells were injected subcutaneously into the right flank of CD1 nude mice. Tumor volume (mm^3) was quantified three times a week by measuring tumor shortest (d) and longest (D) diameters with an electronic caliper, using the formula $D \times d^2/2$. After 17 days from injection, mice were sacrificed, serum were collected to purify exosomes and tumor mass was harvested and weighed. For tail vein metastasis assay, $1x10^6$ of HCT116 cells, treated with Exo Mock and Exo *Alu* RNA for 24 hours were injected intravenously via tail vein of CD1 nude mouse (n = 8 mice per group) Four weeks after the injection, the lungs were explanted and the sera were collected to purify exosomes.

Immunohistochemical staining

Mice lungs were fixed in 4% PFA and paraffin embedded. Immunostaining was performed on 7 µm thick sections. Antigen retrieval was performed for 15 minutes at 37°C in 0.2% trypsin, 0.001% $CaCl_2$ solution. Endogenous peroxidase activity was blocked with a 0.3% H_2O_2 for 30 minutes. After the blocking with 10% goat serum, 1% BSA in PBS/0.1% Triton-X-100, slides were stained using primary antibody Anti-Human Nuclei Antibody, clone 3E1.3 (Merck - Sigma-Aldrich, 1:200) for 16 hours at 4°C. Then, the slides were stained with Goat-Anti-Mouse Biotinylate (DAKO) followed by the signal amplification performed using Vectastain elite ABC kit (Vector Laboratories). The signal was visualized using an ultraView Universal DAB Detection Kit (Merck - Sigma-Aldrich). The slides were counterstained with hematoxylin. All counts were performed on five different randomly fields on at least four random sections for each animal. All images were recorded with a digital cameraLeica DC480 (Leica).

Statistical analysis

Data are expressed as mean ± SEM, with $p < 0.05$ considered statistically significant. Differences among groups were tested by one-way ANOVA.

Results

Alu RNA induces EMT through NLRP3 inflammasome activation in CRC cell lines

We previously demonstrated that *Alu* RNA induces EMT in SW480 colorectal cancer cell without affecting cell proliferation [14]. In contrast, other reports have shown that *Alu* RNA has a cytotoxicity effect on other cancer cell lines [6,10,11]. To better understand the role of *Alu* retroelements and the downstream activated pathways in CRC progression, we tested the effect of *Alu* RNA overexpression in different CRC cell lines by transfecting them with a synthetically transcribed RNA. As shown in Fig. 1a, *Alu* RNA induced a cytotoxic effect in two CRC cell lines (HCT116 and LS174T), as well as other cancer cell lines, independently from their tissue of origin, such as kidney (A498), lung (H460), cervix (HeLa), and breast (MCF7) (**Supplementary Fig. S1**). Conversely, *Alu* RNA did not alter the cell viability of both HT29 and SW480 CRC cells lines, the latter in accordance with our previous report [14] (Fig. 1a). In line with these results, western blot analysis revealed an increase of Caspase-3 cleavage only in *Alu*-sensitive (HCT116 and LS174T) but not in *Alu*-resistant (HT29 and SW480) CRC cell lines (**Supplementary Fig. S2**).

We support the idea that *Alu* RNAs promote CRC progression, despite the fact that these sequences are cytotoxic in most of cancer cell lines. Since the amount of *Alu* RNA in pathophysiological context is extremely low compared to what we transfected *in vitro*, we decided to study dose-dependent effects of transfected *Alu* RNA on HCT116 cell lines. Interestingly, we found that this mechanism is finely-tuned. Indeed, as shown in Fig. 1b, high doses of *Alu* RNA induced cytotoxicity in HCT116 cells, whereas low doses of *Alu* RNA, which are about thirty times less than the amount we transfected, are able to induce a slight but significant increase in HCT116 cell viability.

Since *Alu* RNA has been shown to activate the NLRP3 inflammasome[6], we interrogated whether this pathway is also activated in CRC cells. Interestingly, we found that both high and low doses of *Alu* RNA induce inflammasome priming in HCT116 by upregulating the expression of *NLRP3* and *IL-1B* mRNA, while no change in *IL18* was observed, as evaluated by qRT-PCR (**Supplementary Fig. S3**). Additionally, both doses of *Alu* RNA activated the NLRP3 inflammasome, leading to Caspase-1 activation and the release of IL-1β as measured by western blot (Fig. 1c) and ELISA (Fig. 1d), respectively. Next, we investigated whether *Alu* RNA induces EMT in HCT116 cells, as we had previously demonstrated in SW480 cells [14]. As shown in Fig. 1c, western blot analysis showed how both high and low doses of *Alu* RNA induce EMT in HCT116, as evidenced by the downregulation of E-cadherin expression and upregulation of Fibronectin, Vimentin and ZEB1, an EMT-transcription factor that is strongly induced by *Alu* RNA. Consistent with these findings, immunofluorescence analyses confirmed that both high and low doses of *Alu* RNA promoted cytoskeleton reorganization (Fig. 1e). Collectively, these data suggests that, even in minimal amounts, *Alu* RNA is able to activate NLRP3 inflammasome and to promote EMT in HCT116 cell line.

Since IL-1b has been shown to induce EMT in cancer [20,21], we hypothesized that *Alu* RNA could induce EMT through NLRP3 inflammasome activation. To test this hypothesis, we performed a rescue experiment transfecting the HCT116 cell line with a siRNA targeting *NLRP3* mRNA before introducing *Alu* RNA. As control, a siRNA against *Luciferase* mRNA was used. As shown in Fig. 1f, si*NLRP3* efficiently

reduced *NLRP3* expression in HCT116 cells, as assessed by qRT-PCR. Next, we monitored the expression levels of the EMT markers by western blot, once inflammasome activation was impaired. Consistent with previous data, our results confirmed that *Alu* RNA (central lane, Fig. 1g) induces Caspase-1 cleavage, as well as EMT, reducing E-cadherin levels and increasing the expression of mesenchymal markers (Fibronectin, Vimentin and ZEB1) compared to Mock (left lane, Fig. 1g). Surprisingly, the transfection of *Alu* RNA in si*NLRP3* transfected cells rescued the *Alu*-induced EMT through a reduction of Caspase-1 activation (right lane, Fig. 1g). F-Actin staining confirmed that the knockdown of *NLRP3* prevented the mesenchymal phenotype induced by *Alu* RNA (Fig. 1h). In accordance with this data, we found that pharmacological inhibition of NLRP3 with dapansutrile (OLT1177) [23] also reduced EMT induced by *Alu* RNA as a consequence of impaired NLRP3 inflammasome activation (**Supplementary Fig. S4**). Next, we investigated whether NLRP3 inflammasome is also activated in SW480 cells, in which we demonstrated that *Alu* RNA induced EMT, but we were not able to detect either cleavage of Caspase-1 or secretion of interleukins-1b/18 by western blot [14]. In lane with these results, we found that *Alu* RNA was able to prime the NLRP3 inflammasome (**Supplementary Fig. S5a**) and trigger a slight but significant increase of Caspase-1 activation, as determined with a fluorometric assay (**Supplementary Fig. S5b**), further supporting that EMT is downstream the inflammasome. Collectively, these data demonstrate that *Alu* RNA induces EMT through the activation of NLRP3 inflammasome and the release of IL-1b in CRC cells.

AluRNA is transported by exosomes in CRC cells

Retrotransposon elements, such as *Alu* sequences, are enriched in tumors-derived exosomes [15], thus we investigated whether *Alu* RNA could promote CRC progression by moving through exosomes since. To address this question, *in vitro* transcribed *Alu* RNA was transfected in the SW480 CRC cell line and exosomes were isolated from culture supernatant of SW480/*Alu* RNA and control cells (SW480/Mock) by a combination of centrifugations and ultracentrifugations. The purified exosomes were identified and characterized by transmission electron microscopy (TEM), dynamic light scattering (DLS) and western blot analysis. Exosomes purified from conditional media of SW480 were identified as membrane-encapsulated particles with a range of 100 to 130 nm in size by TEM (Fig. 2a). Dynamic light scattering (DLS) analysis in **Supplementary Figure S6** revealed that the exosome preparations from SW480/*Alu* RNA and SW480/Mock were homogenous in size distribution. Western blot analysis revealed that the vesicles were positive for exosome marker CD63 (Fig. 2b). Finally, we analyzed total RNA isolated from exosomes for the presence of *Alu* transcripts. qRT-PCR analysis showed a significant accumulation of *Alu* transcripts in exosomes derived from SW480/*Alu* RNA compared to exosomes derived from control cells (Fig. 2c). This result was further confirmed by northern blot analysis where the presence of a faster band that correspond to the exogenous and transfected *Alu* RNA is also clearly evident (Fig. 2d**)**. As control the same analyses were carried out on non-transfected cells (Figs. 2c and 2d**)**. Next, SW480 and HCT116 cells were incubated with PKH67-labeled exosomes derived from SW480 and as shown in Fig. 2e both CRC cells lines are able to internalize exosomes. These results clearly demonstrate that Pol III-derived *Alu* transcripts are stored and transported by exosomes in CRC cells.

Cancer-derived exosomal- Alu RNA promotes tumorigenesis

We then investigated whether *Alu* RNA could be transferred via exosomes in HCT116 and SW480 cells. Exosomes derived from SW480/Mock (Exo Mock) and SW40/*Alu* RNA (Exo *Alu*) were co-cultured with HCT116 cells at different time points. As shown by qRT-PCR analysis in Fig. 3a, an increase in *Alu* RNA was observed after 16 hours of incubation, with a peak at 24 hours and still sustained at 48 hours in HCT116 compared to untreated cells and cells incubated with Exo Mock. Similar kinetics of expression were also observed when SW480-derived exosomes were co-cultured with SW480 cells (**Supplementary Fig. S7**), thus indicating that exosomal-*Alu* RNA can be transferred in recipient cells.

Next, we tested whether exosomal-*Alu* RNA could affect CRC cell viability. Interestingly, we did not observe significant effects on HCT116 and SW480 cell growth, as shown in Fig. 3b and **Supplementary Fig. 8a**. Consistent with this finding, plate colony-formation assays revealed no difference in growth between HCT116 and SW480 treated with exosomes enriched in *Alu* RNA (Exo *Alu* RNA) compared to cells treated with Exo Mock, as shown in Fig. 3c and **Supplementary Fig. 8b**. Interestingly, we found that exosomes enriched in *Alu* RNA significantly promoted invasion and increased the ability to grow in anchorage-independent manner of HCT116 and SW480 cells, as compared to cells treated with control exosomes (Fig. 3d, e and **Supplementary Fig. 9a, b**, respectively), indicating that the transfer of *Alu* transcripts in CRC cells promotes a pro-tumoral phenotype in *in vitro* cell-based assays.

Finally, we tested the ability of exosomal-*Alu* RNA to increase the cell metastatic potential *in vivo*. HCT116 cells were co-cultured with exosomes enriched in *Alu* RNA or control exomes for 24 hours before being intravenously injected into the tail vein of immunocompromised CD1 mice. After four weeks, the lungs were explanted and the ability of cells to invade pulmonary tissue was evaluated by immunohistochemical analysis using an antibody that specifically recognizes human nuclei. Interestingly, we found that the lungs of mice injected with cells pre-treated with Exo *Alu* significantly contained more positive nuclei than those injected with cells pre-treated with control exosomes (Fig. 3f**)**. It is noteworthy that all lungs explanted from mice in the Exo *Alu* group showed positivity to anti-human nuclei antibody, while one third of the lungs in the control group did not show any positivity to the antibody. This further indicates that exosomal-*Alu* RNA confers an increased metastatic potential to HCT116 cells. Collectively these data demonstrated that cancer-derived exosomal-*Alu* RNA induces tumorigenesis and promote metastasis dissemination.

Exosomal-AluRNA induces tumorigenesis via NLRP3 inflammasome activation

We then evaluated whether the activation of the NLRP3 inflammasome and the induction of EMT were involved in the ability of exosomal-*Alu* RNA to promote tumorigenesis in CRC cells. Exosomal-*Alu* RNA induced inflammasome priming by upregulating *NLRP3* and *IL-1B* mRNAs in comparison to cells treated with control exosomes. This occurred equivalently in both HCT116 and SW480 CRC cell lines, as shown in Fig. 4a and **Supplementary Figure S10a**, respectively. Consistent with this result, we observed Caspase-1 activation, as assessed by western blot analysis in HCT116 cells (Fig. 4b) and by flow cytometry analysis in SW480 cells (**Supplementary Fig. S10b**). Next, we assessed whether exosomal-*Alu* RNA promoted EMT in these cells. As shown in Fig. 4c, we observed a decrease in the epithelial marker E-

Cadherin, an increase in the mesenchymal markers, Fibronectin and Vimentin, as well as an increase of transcription factor ZEB1 in HCT116 cells treated with Exo *Alu* RNA, as assessed by western blot. These changes are reflected in the acquisition of a mesenchymal phenotype in HCT116 treated with Exo *Alu* RNA, as shown by the immunofluorescence analysis with F-Actin. Similarly, exosomal-*Alu* RNA induced a mesenchymal phenotype in SW480 cells, as shown by western blot analysis (**Supplementary Fig. S11**). Consistent with previous data, we found that dapansutrile (OLT1177) inhibited the ability of Exo *Alu* RNA to promote HCT116 cell invasion (Fig. 4d). Collectively, these data indicate that the activation of the NLRP3 inflammasome is a critical mediator of the ability of exosomal-*Alu* RNA to induce tumorigenesis.

Next, we tested whether human CRC tumors that exhibit an accumulation of *Alu* RNA, which was associated with progression and malignancy [14], also displayed evidence of inflammasome activation. The abundance of *NLRP3* and *IL1B* mRNAs was quantified in 13 matched non-tumoral tissues (NT), primary colon tumor (T) and liver metastasis (M) compared with non-tumoral tissues (NT). Interestingly, we found that both *NLRP3* and *IL1B* mRNAs are significantly upregulated in both primary colon tumor (T) and in liver metastasis (M) compared with non-tumoral tissues (NT) (Fig. 4e). These data provide evidence that *Alu* RNA accumulation in human CRC tumors determines a priming of inflammasome, mirroring the functional data obtained in cell culture studies.

Exosomal- Alu RNA abundance correlates with CRC progression

Since one of the major applications of exosomes is diagnosis, we investigated whether abundance of *Alu* RNA could be potentially used as cancer biomarkers. Therefore, we analyzed whether the exosomal-*Alu* RNA content correlated with malignancy *in vivo*. We isolated RNA from exosomes purified from the serum of xenotransplanted mice with human colorectal cancer cells bearing large and small tumors. As shown in the northern blot in Fig. 5a, we observed an increased accumulation of *Alu* transcripts in exosomes derived from the serum of mice bearing large tumors compared to those bearing small tumors. Moreover, this result was confirmed by a second and independent experiment in which we analyzed the abundance of exosomal-*Alu* RNA in each mouse by qRT-PCR analysis. As shown in Fig. 5b, we observed a significant increase in the amount of exosomal-*Alu* RNA in large tumors compared to small tumors, as normalized on human *18S*. Furthermore, we analyze the abundance of *Alu* RNA in exosomes derived from serum of mice in which we intravenously injected HCT116 pre-treated with exosomes enriched in *Alu* RNA (Fig. 3f) to assess whether exosomal-*Alu* RNA content correlates with metastasis *in vivo*. Interestingly, we found a significative increase in *Alu* transcripts in the exosomes isolated from mice injected with Exo *Alu* RNA treated cells when compared to control (Fig. 5c).

Collectively, these data clearly show that exosomal-*Alu* RNA content correlates with CRC progression *in vivo* and that these transcripts could be potentially used as cancer biomarkers.

Discussion

Our data define the molecular mechanism by which Pol III-derived *Alu* transcripts promote the progression of colorectal cancer. We show that cancer-derived exosomal-*Alu* RNA can be delivered to CRC cells and

promotes cancer progression by inducing EMT through NLRP3 inflammasome activation. Furthermore, we find that the abundance of *Alu* transcripts in exosomes correlated with CRC progression in preclinical models. Collectively, our study reveals the direct involvement of *Alu* RNA retroelements in cancer pathogenesis and their clinical significance.

We have found that *Alu* RNA plays a dual and opposing role in regulating CRC cell fate. Consistent with previous reports [5,10,11,14], we found that the transfection of *in vitro* transcribed *Alu* RNA can either cause cell death or have no effect on cell viability. This variability could be attributed to different concentration of *Alu* RNA accumulation as well as to differences in mutations on tumor suppressor genes in the cancer cell lines analyzed. Therefore, future studies should aim to better determine the molecular mechanisms underlying these differences. However, we found that the signal transduction downstream is the same in both *Alu*-sensitive and *Alu*-resistant CRC cell lines, even when the amount of transfected *Alu* RNA is extremely low.

Furthermore, both high and low doses of *Alu* RNA induce NLRP3 inflammasome activation in CRC cell lines, leading to the secretion of IL-1β. In the case of high dose, this leads to cell death, whereas in the case of low dose a slight but significant induction of proliferation occurs. The secretion of IL-1β has been shown to occur upon cell death due to the membrane plasma ruptures [24] or by pyroptosis, a lytic form of cell death triggered by the activation of Caspase-1 [25], yet a recent study has demonstrated that cell death is not essential for Caspase-1-mediated IL-1β activation and secretion [26], which is likely what is happening in CRC cells.

Due to its broad activity in shaping immune response the role of NLRP3 inflammasome in CRC development is complex and controversial, as it has been reported to have both protective and promoting effects on tumorigenesis. The protective role of NLRP3 inflammasome in colitis-associated colon cancer has been well established since it helps to resolve inflammation and prevent the development of cancer [27]. However, chronic inflammation can also promote carcinogenesis, and the activation of NLRP3 inflammasome has been linked to numerous human malignancies, including CRC. Genetic variants in the *NLRP3* gene has been associated with an increased risk of colon cancer [28], and NLRP3 inflammasome activation is increased in CRC human tissues. This activation is associated with increased production of IL-1β and it has been also linked to EMT process and cancer progression [18,19]. In this context, *Alu* RNA trafficking through exosomes could be one of the stimuli that could activate the NLRP3 inflammasome in CRC.

We demonstrated that exosomal-*Alu* RNA promotes tumorigenesis by inducing NLRP3 inflammasome activation and EMT in CRC cells lines. Our findings are supported by the analysis of human CRC tumors, in which we have previously found that *Alu* RNAs expression correlates with progression and metastasis[14]. Here, we observed that the accumulation *of Alu* RNA in CRC human tissues is associated with the priming of NLRP3 inflammasome. Although further studies are needed in order to clarify the molecular mechanism underlying *Alu* RNA-induced inflammasome activation in CRC cells, these results strongly suggests that inflammasome activation occurs *in vivo*.

Interestingly, a recent study reveals that colorectal cancers express abundant repetitive elements, including long interspersed nuclear element-1 (LINE-1) retrotransposons, *Alu* RNAs and satellite repeats. These transposable elements have a viral-like cycle that can be therapeutically targeted with nucleoside reverse transcriptase inhibitors (NRTIs), thus preventing CRC progression in pre-clinical models [29]. Notably, we showed that NRTIs are able to inhibit *Alu* RNA-mediated signaling through inhibition of P2X7-mediated NLRP3 inflammasome activation, independently of reverse transcriptase inhibition [30]. In this context, our study confirms and reinforces the importance of *Alu* repetitive elements in CRC progression and provide another potential therapeutic strategy. Furthermore, it has been recently demonstrated that fluoxetine, an FDA-approved drug for the treatment of clinical depression, that has been identified to bind and inhibit NLRP3 and of consequences *Alu* RNA-dependent signaling [31] increase the overall survival of cancer patients treated with PD-1/L1 immunotherapy [32], thus underlining the importance of NLRP3 signaling in cancer.

Exosomes have been shown to transfer their cargos from donor to recipient cells and be responsible for cancer-induced vascular permeability, inflammation, formation of pre-metastasis niche [33,34]. In this manuscript, we studied how exosomal-*Alu* RNA affects CRC cell behavior, but this does not exclude the possibility that the transfer of these transcripts could affect other non-cancer cells, that are part of the tumor microenvironment, such as endothelial cells, inflammatory cells, and fibroblasts. Since inflammatory cells, such as macrophages, express high levels of NLRP3, this area of investigation will be particularly intriguing.

Recent studies reveal the emerging role of exosomes derived from the cancer patient's serum as reliable markers for cancer diagnosis and prognosis assessment. Tumor microvescicles have been found to contain retrotransposons elements, such as LINE-1 and *Alu* elements [15]. Here we show that, in preclinical tumor model, *Alu* abundance in exosomes isolated from the serum is associated with tumor progression and could be potentially used as a marker for cancer diagnosis.

In conclusion, our findings reveal that *Alu* transcripts transferred through exosomes are able to positively affect colorectal cancer progression by activating NLRP3 inflammasome, thus providing new insights into the importance of *Alu* sequences in cancer progression and opening new horizons for diagnostic e therapeutic strategies.

Declarations

Funding information: Italian Ministry of University and Research (PRIN 2020FR7TCL), EU funding within the MUR PNRR "National Center for Gene Therapy and Drugs based on RNA Technology" (Project no. CN00000041 CN3 RNA).

Aknowledegments

The authors thank Marinella Pirozzi of the EuroBioimaging facility located in IEOS-CNR (Castellino campus) for providing access to the imaging instruments used in this study. The IGB integrated microscopy and FACS facilities for technical assistance. Menotti Ruvo and Annamaria Sandomenico for providing access to Dynamic Light Scattering instrument. This work was supported by Italian Ministry of University and Research (PRIN 2020FR7TCL) to V.T. and by EU funding within the MUR PNRR “National Center for Gene Therapy and Drugs based on RNA Technology” (Project no. CN00000041 CN3 RNA) to S.D.F. The Eurobioimaging facility is supported by the following grants: PON-IMPARA, SEELIFE and CIRO.

References

1. Deininger, P. Alu elements: know the SINEs. *Genome Biol* 12, 236 (2011).
2. Batzer, M. A. & Deininger, P. L. Alu repeats and human genomic diversity. *Nat Rev Genet* 3, 370–379 (2002).
3. Häsler, J., Samuelsson, T. & Strub, K. Useful ‘junk’: Alu RNAs in the human transcriptome. *Cell Mol Life Sci* 64, 1793–1800 (2007).
4. Burns, K. H. Repetitive DNA in disease. *Science* 376, 353–354 (2022).
5. Kaneko, H. *et al.* DICER1 deficit induces Alu RNA toxicity in age-related macular degeneration. *Nature* 471, 325–330 (2011).
6. Tarallo, V. *et al.* DICER1 loss and Alu RNA induce age-related macular degeneration via the NLRP3 inflammasome and MyD88. *Cell* 149, 847–859 (2012).
7. Hung, T. *et al.* The Ro60 autoantigen binds endogenous retroelements and regulates inflammatory gene expression. *Science* 350, 455–459 (2015).
8. Ambati, J. *et al.* Repurposing anti-inflammasome NRTIs for improving insulin sensitivity and reducing type 2 diabetes development. *Nat Commun* 11, 4737 (2020).
9. Pascarella, G. *et al.* Recombination of repeat elements generates somatic complexity in human genomes. *Cell* 185, 3025-3040.e6 (2022).
10. Baryakin, D. N. *et al.* Alu- and 7SL RNA Analogues Suppress MCF-7 Cell Viability through Modulating the Transcription of Endoplasmic Reticulum Stress Response Genes. *Acta Naturae* 5, 83–93 (2013).
11. Sakamoto, K., Fordis, C. M., Corsico, C. D., Howard, T. H. & Howard, B. H. Modulation of HeLa cell growth by transfected 7SL RNA and Alu gene sequences. *J Biol Chem* 266, 3031–3038 (1991).
12. Zhao, Y. *et al.* Transposon-triggered innate immune response confers cancer resistance to the blind mole rat. *Nat Immunol* 22, 1219–1230 (2021).
13. Tang, R.-B. *et al.* Increased level of polymerase III transcribed Alu RNA in hepatocellular carcinoma tissue. *Mol Carcinog* 42, 93–96 (2005).
14. Di Ruocco, F. *et al.* Alu RNA accumulation induces epithelial-to-mesenchymal transition by modulating miR-566 and is associated with cancer progression. *Oncogene* 37, 627–637 (2018).
15. Balaj, L. *et al.* Tumour microvesicles contain retrotransposon elements and amplified oncogene sequences. *Nat Commun* 2, 180 (2011).

16. Kantono, M. & Guo, B. Inflammasomes and Cancer: The Dynamic Role of the Inflammasome in Tumor Development. *Front Immunol* 8, 1132 (2017).
17. Schroder, K. & Tschopp, J. The inflammasomes. *Cell* 140, 821–832 (2010).
18. Marandi, Y. *et al.* NLRP3-inflammasome activation is associated with epithelial-mesenchymal transition and progression of colorectal cancer. *Iran J Basic Med Sci* 24, 483–492 (2021).
19. Shao, X., Lei, Z. & Zhou, C. NLRP3 Promotes Colorectal Cancer Cell Proliferation and Metastasis via Regulating Epithelial Mesenchymal Transformation. *Anticancer Agents Med Chem* 20, 820–827 (2020).
20. Li, R. *et al.* Chronic IL-1β-induced inflammation regulates epithelial-to-mesenchymal transition memory phenotypes via epigenetic modifications in non-small cell lung cancer. *Sci Rep* 10, 377 (2020).
21. Li, Y., Wang, L., Pappan, L., Galliher-Beckley, A. & Shi, J. IL-1β promotes stemness and invasiveness of colon cancer cells through Zeb1 activation. *Mol Cancer* 11, 87 (2012).
22. Tulotta, C. *et al.* Endogenous Production of IL1B by Breast Cancer Cells Drives Metastasis and Colonization of the Bone Microenvironment. *Clin Cancer Res* 25, 2769–2782 (2019).
23. Marchetti, C. *et al.* OLT1177, a β-sulfonyl nitrile compound, safe in humans, inhibits the NLRP3 inflammasome and reverses the metabolic cost of inflammation. *Proc Natl Acad Sci U S A* 115, E1530–E1539 (2018).
24. Cullen, S. P., Kearney, C. J., Clancy, D. M. & Martin, S. J. Diverse Activators of the NLRP3 Inflammasome Promote IL-1β Secretion by Triggering Necrosis. *Cell Rep* 11, 1535–1548 (2015).
25. Fink, S. L. & Cookson, B. T. Caspase-1-dependent pore formation during pyroptosis leads to osmotic lysis of infected host macrophages. *Cell Microbiol* 8, 1812–1825 (2006).
26. Conos, S. A., Lawlor, K. E., Vaux, D. L., Vince, J. E. & Lindqvist, L. M. Cell death is not essential for caspase-1-mediated interleukin-1β activation and secretion. *Cell Death Differ* 23, 1827–1838 (2016).
27. Zaki, M. H. *et al.* The NLRP3 inflammasome protects against loss of epithelial integrity and mortality during experimental colitis. *Immunity* 32, 379–391 (2010).
28. Ungerbäck, J. *et al.* Genetic variation and alterations of genes involved in NFκB/TNFAIP3- and NLRP3-inflammasome signaling affect susceptibility and outcome of colorectal cancer. *Carcinogenesis* 33, 2126–2134 (2012).
29. Rajurkar, M. *et al.* Reverse Transcriptase Inhibition Disrupts Repeat Element Life Cycle in Colorectal Cancer. *Cancer Discov* 12, 1462–1481 (2022).
30. Fowler, B. J. *et al.* Nucleoside reverse transcriptase inhibitors possess intrinsic anti-inflammatory activity. *Science* 346, 1000–1003 (2014).
31. Ambati, M. *et al.* Identification of fluoxetine as a direct NLRP3 inhibitor to treat atrophic macular degeneration. *Proc Natl Acad Sci U S A* 118, e2102975118 (2021).
32. Magagnoli, J. *et al.* Association between Fluoxetine Use and Overall Survival among Patients with Cancer Treated with PD-1/L1 Immunotherapy. *Pharmaceuticals (Basel)* 16, 640 (2023).

33. Becker, A. *et al.* Extracellular Vesicles in Cancer: Cell-to-Cell Mediators of Metastasis. *Cancer Cell* 30, 836–848 (2016).

34. Wortzel, I., Dror, S., Kenific, C. M. & Lyden, D. Exosome-Mediated Metastasis: Communication from a Distance. *Dev Cell* 49, 347–360 (2019).

Figures

Figure 1

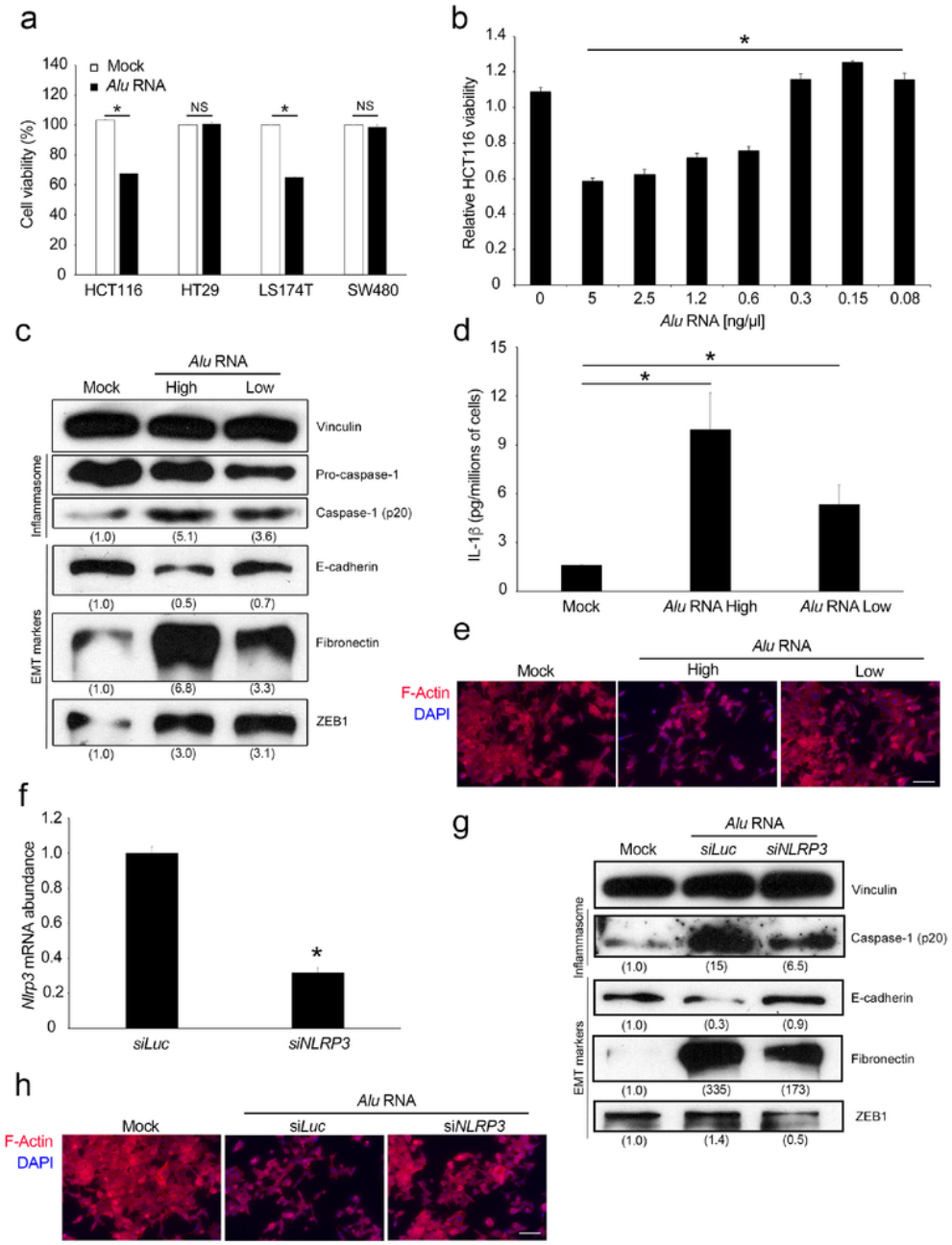

Figure 1

***Alu* RNA induces EMT through NLRP3 inflammasome activation in CRC cell lines. a)** *Alu* RNA induces cytotoxicity in HCT116 and LS174T cells but does not alter viability of HT29 and SW480 cells, as determined by MTT assay (n=3). **b)** Dose-dependent effects of *Alu* RNA on HCT116 cell viability, as monitored by MTT assay (n=3). **c)** Western blot analysis shows the activation of Caspase-1, an increase of the mesenchymal marker (Fibronectin), a decrease of E-cadherin and an increase of the EMT transcription factor ZEB1, after transfection of HCT116 with high and low doses of *Alu* RNA. Densitometric values are normalized against Vinculin and are shown in parentheses. **d)** High and low doses of *Alu* RNA induce secretion of IL-1b from HCT116 cells, as measured by ELISA. IL-1b protein levels were normalized with respect to the number of adherent cells (n=3); **e)**Representative images of HCT116 cells transfected with vehicle (Mock, left), high *Alu* RNA (middle), and low *Alu* RNA (right) stained for F-actin with rhodamine phalloidin (red). Nuclei are counterstained with 4',6-diamidino-2-phenylindole (DAPI, blue). Scale bar: 100 mm. **f)** The transfection of a siRNA targeting *NLRP3* (*siNLRP3*) reduces the abundance of target mRNA in HCT116 cells compared with control siRNA (si*Luc)*, as determined by qRT-PCR (n=3). The transfection of *siNLRP3* rescued *Alu*-induced EMT in HCT116 cells, as determined by **g**) western blot and by **h**) immunofluorescence analyses. *Alu* RNA (central lane, **g**) induces Caspase-1 activation as well as EMT reducing E-cadherin and increasing Fibronectin and ZEB-1 compared to Mock (left lane, **g**). The transfection of *Alu* RNA in *siNLPR3* silenced cells rescues the *Alu*-induced EMT inhibiting *Alu*-induced Caspase-1 activation (right lane, **g**). Densitometric values are normalized against Vinculin and are shown in parentheses. **h**) Representative images of F-actin (red) staining. Nuclei are counterstained with DAPI (blue). Scale bar: 100 mm. For all panels, *p<0.05; NS= not statistically significant. Error bars denote s.e.m.

Figure 2

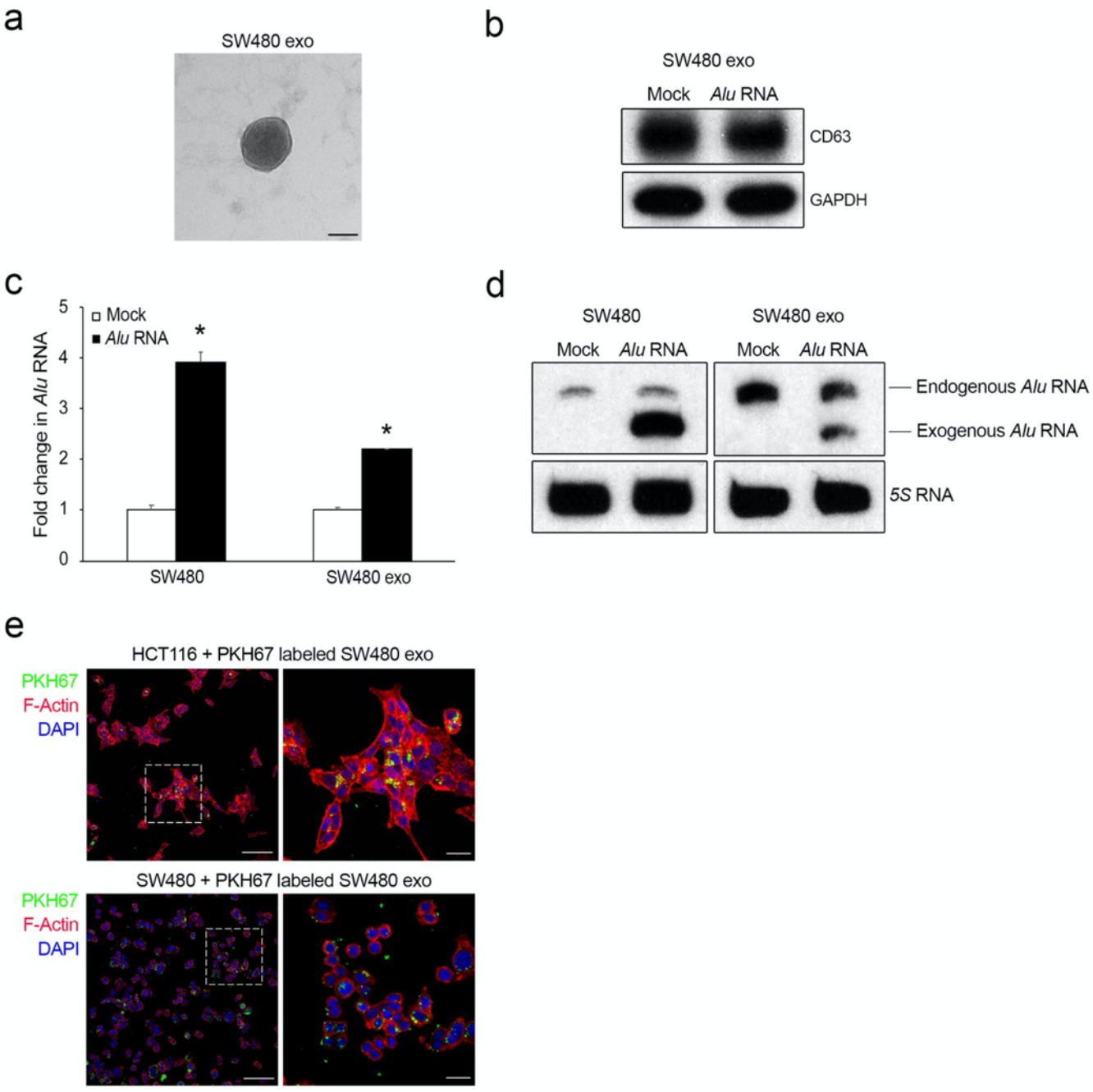

Figure 2

***Alu* RNA is stored and transported by exosomes in CRC cells. a)** Electron microscopy shows vesicles with characteristic morphology and size of exosomes. Scale bar: 50 nm. **b)** Western blot analysis for CD63 of exosomes purified by ultracentrifugation from culture supernatant of SW480 cells (SW480 exo) transfected with *Alu* RNA and with vehicle (Mock). GAPDH is used as loading control. **c)** qRT-PCR shows *Alu* RNA abundance in exosomes derived from SW480 cells (SW480 exo) transfected with *Alu* RNA as

compared to vehicle-transfected cells (Mock). On the left, as control, the same analysis was performed on SW480 cells transfected with *Alu* RNA and vehicle (Mock) (n=3); *p<0.05. Error bars denote s.e.m. **d)**Northern blot analysis shows *Alu* RNA abundance in exosomes derived from SW480 cells (SW480 exo) transfected with *Alu* RNA as compared to vehicle-transfected cells (Mock). On the left, as control, the same analysis was performed on SW480 cells transfected with *Alu* RNA and vehicle (Mock). We observed the band of endogenous *Alu* RNA (around 300 nucleotides long) and a faster band that corresponded to the transfected exogenous *Alu* RNA (281 nucleotides long). *5S* RNA is used as loading control (n=3). **e)** Representative confocal images of PKH67 labeled SW480-derived exosomes (green) in HCT116 and SW480 cells stained for F-actin with rhodamine phalloidin (red). Nuclei are counterstained with DAPI (blue). Scale bar: 100 mm. A higher magnification is shown on the right. Scale bar: 25 mm.

Figure 3

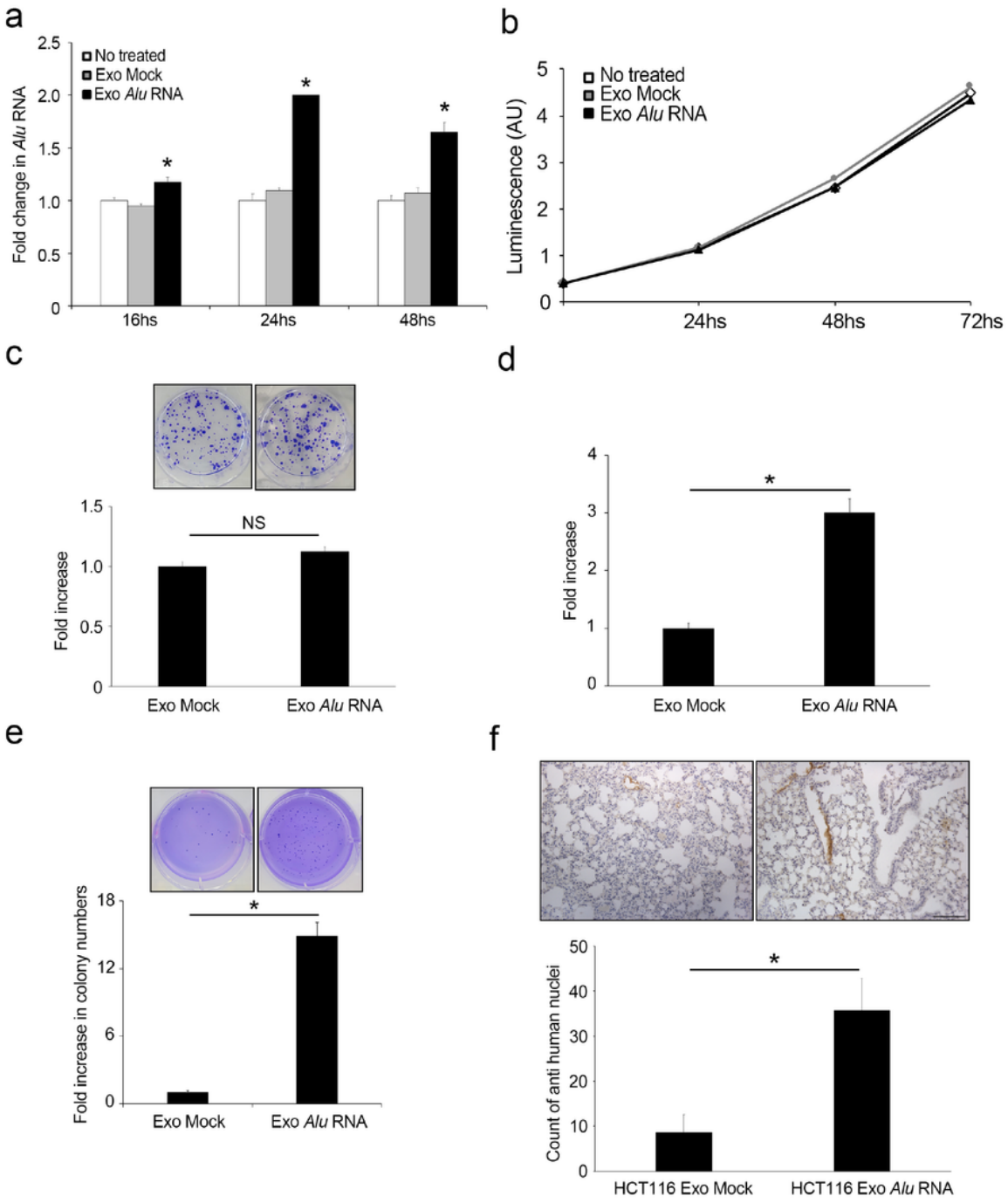

Figure 3

Cancer-derived exosomal-*Alu* RNA promotes tumorigenesis and metastasis dissemination. a) qRT-PCR shows *Alu* RNA abundance in HCT116 cells treated with exosomes derived from *Alu*-transfected SW480 (Exo *Alu* RNA) after 16, 24 and 48 hours as compared with HCT116 cells treated with control exosomes (Exo Mock) and untreated cells (n=3); *p<0.05. Error bars denote s.e.m. **b)** Exosomal-*Alu* RNA does not alter HCT116 cell viability over time, as monitored by luminescent assay (n=3). **c)** Exosomal-*Alu* RNA

does not alter the ability of HCT116 to form colonies. Data are expressed as fold increase with the respect to HCT116 treated with Exo Mock (n=3). Error bars denote s.e.m. Representative pictures of the two conditions are shown. **d)** Exosomal-*Alu* RNA increases HCT116 cell invasion. Data are expressed as fold increase with the respect to HCT116 treated with Exo Mock (n=3); *p=0.019. Error bars denote s.e.m. **e)**Exosomal-*Alu* RNA increases HCT116 ability to grow in anchorage-dependent manner. The bars indicate the average of colony numbers in each well (n=3); *p=0.001. Error bars denote s.e.m. Representative pictures of two conditions are shown. **f)** Exosomal-*Alu* RNA increases the metastatic potential of HCT116 *in vivo*. The bars indicate the average of numbers of human positive cell nuclei counted in lung sections from tail-vein injected mice with HCT116 cells treated with Exo *Alu* RNA as compared to Exo Mock-injected mice; *p=0.012. Error bars denote s.e.m. Representative pictures of anti-human nuclei staining of lung sections are shown. Scale bar: 100 μm

Figure 4

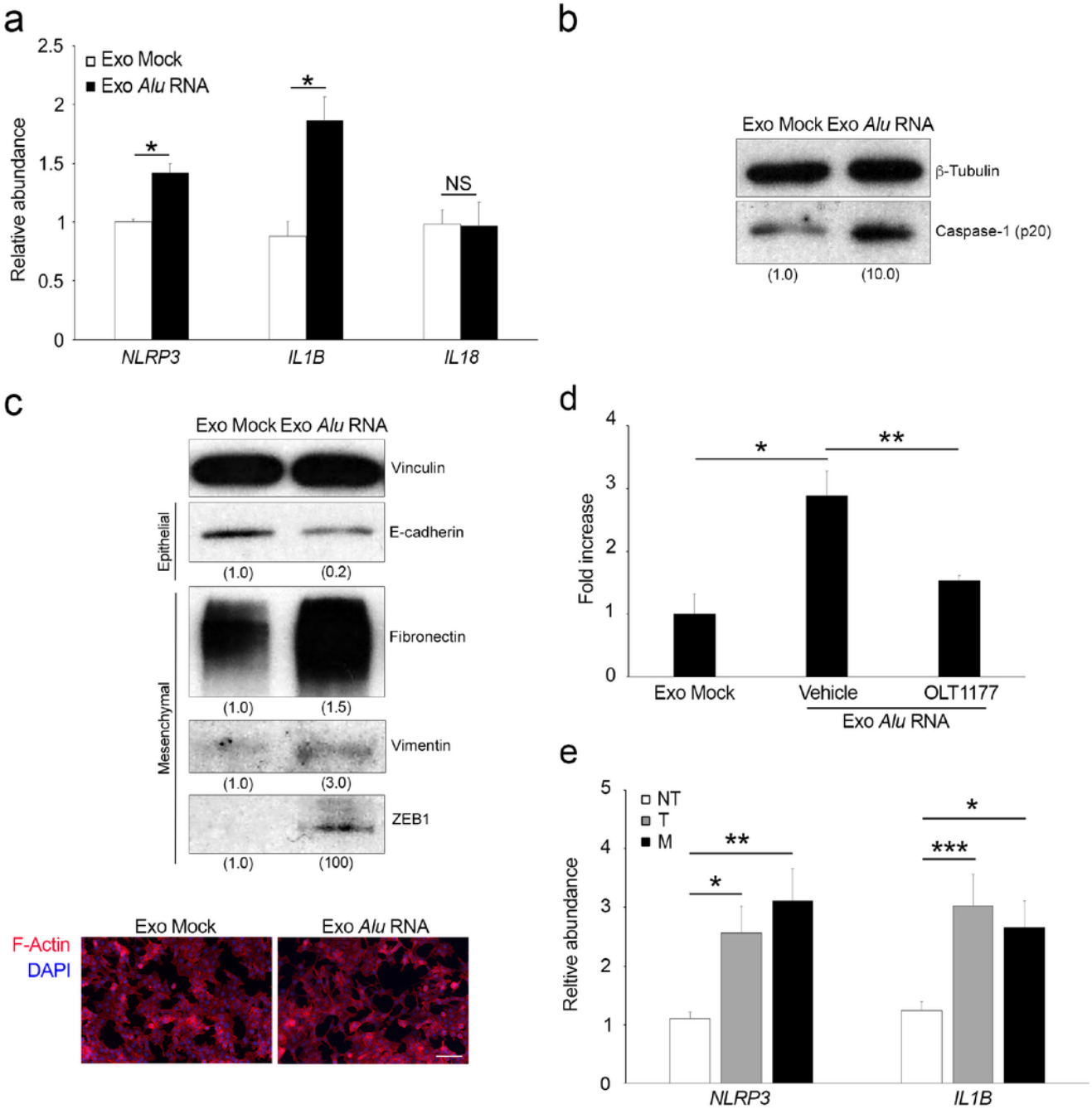

Figure 4

Exosomal-*Alu* RNA induces tumorigenesis via NLRP3 inflammasome activation. a) Exosomal-*Alu* RNA induces the priming of the NLRP3 inflammasome by increasing the abundance of *NLRP3* and *IL-1B* mRNAs in HCT116 cells, as evaluated by qRT-PCR; (n=3) *p<0.05. No difference in *IL18* gene expression were observed. Error bars denote s.e.m. **b)** Western blot analysis shows the activation of Caspase-1 (p20) in HCT116 cells treated with Exo *Alu* RNA. Densitometric values are normalized against b-Tubulin and are

shown in parentheses. **c)**Western blot analysis (above) shows a decrease of E-cadherin, an increase of the mesenchymal marker (Fibronectin and Vimentin), and of the EMT-TF, ZEB1 in HCT116 cells treated with Exo *Alu* RNA. Densitometric values are normalized against Vinculin and are shown in parentheses. Below, representative images of HCT116 cells treated with Exo Mock and Exo *Alu* RNA stained for F-actin (red). Nuclei are counterstained with DAPI (blue). Scale bar: 100 mm. **d)** OLT1177 (100μM) reduces exosomal *Alu* RNA-induced HCT116 cell invasion. Data are expressed as fold increase with the respect to HCT116 treated with Exo Mock (n=3); *p=0.015; **p=0.027. Error bars denote s.e.m. **f)** *NLRP3* and *IL-1B*mRNAs expression in non-tumoral tissue (NT), primary colon tumor (T) and liver metastasis (M) of 13 matched patients, as evaluated by qRT-PCR and normalized to *18S* mRNA; *p=0.03; **p=0.014; ***p=0.019. Error bars denote s.e.m.

Figure 5

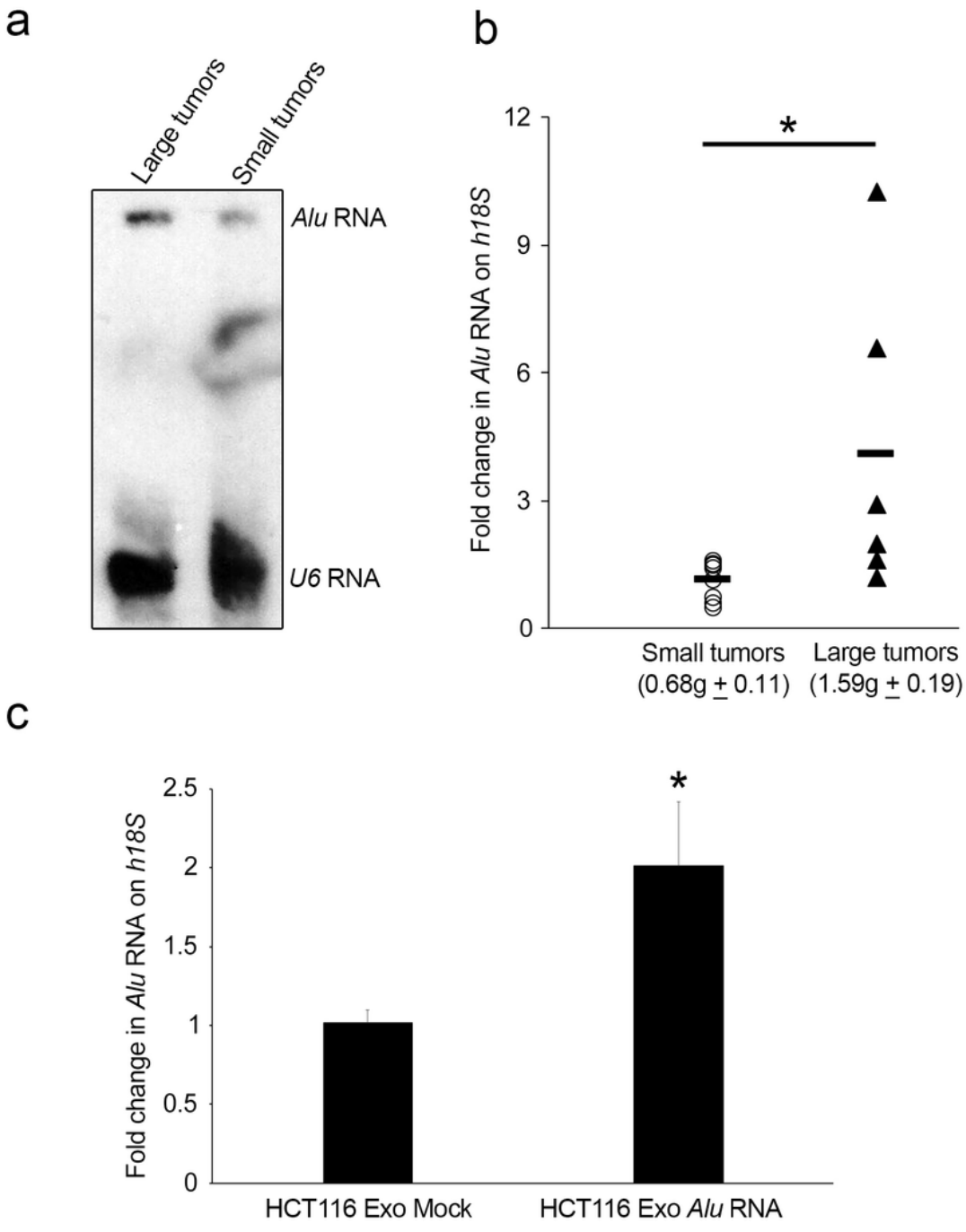

Figure 5

Exosomal-*Alu* RNA abundance correlates with CRC progression. **a)** Northern blot analysis shows *Alu* RNA abundance in exosomes purified by ultracentrifugation from serum of xenotransplanted mice with colorectal cancer cells bearing large (n=8; 1.52±0.09) and small tumors (n=6; 0.88±0.14). *U6* RNA is used as loading control. **b)** qRT-PCR analysis shows *Alu* RNA expression in exosomes purified from serum of each xenotransplanted mice with colorectal cancer cells bearing small (n=8; 0.68g±0.11) and large (n=6;

1.58g±0.19) tumors, as evaluated by qRT-PCR and normalized against human *18S* mRNA; *p=0.037. **c)** qRT-PCR analysis shows *Alu* RNA expression in exosomes purified from serum of mice intravenously injected with HCT116 cells treated with Exo *Alu* RNA and Exo Mock, respectively. The values were normalized against human *18S* RNA; *p=0.025. Error bars denote s.e.m.

Supplementary Files

This is a list of supplementary files associated with this preprint. Click to download.

- MagliacaneTrottaetal.Supplementary.pdf